Investigation of electronic structure, magnetic stability, spin coupling, and thermodynamic properties of novel antiferromagnets XMn_2Y_2 (X = Ca, Sr; Y = P, As)

Zeshan Zada[a], Rifaqat Zada[b], Abdul Ahad Khan[c], Muhammad Saqib[d], Muhammad Fazal Ur Rehman[e], Muhammad Ismail[f], Neeraj Kulhari[g], Krishna Swaroop Sharma[g], Muhammad Ismail[h], Xingchen Shen[i], Muhammad Faizan[c,j,*]

[a] *Materials Modelling Lab, Department of Physics, Islamia College University, Peshawar, Pakistan*
[b] *Departmentof Chemistry, University of Peshawar, KP, Pakistan*
[c] *Department of Physics, University of Peshawar, KP, Pakistan*
[d] *Department of Electrical and Computer Engineering, COMSATS University Islamabad, Abbottabad Campus, KP, Pakistan*
[e] *Department of Chemistry, Lahore Garrison University, Lahore, Pakistan*
[f] *Department of Chemistry, Woman University Swabi, KP, Pakistan*
[g] *Department of Physics, IIS (Deemed to be University), Jaipur, Rajasthan 302020, India*
[h] *School of Environment and Chemical Engineering, North China Electric Power University, Beijing 102206, China*
[i] *Institute for Quantum Materials and Technologies, Karlsruhe Institute of Technology, Karlsruhe 76021, Germany*
[j] *State Key Laboratory of Superhard Materials and School of Materials Science and Engineering, Jilin University, Changchun 130012, China*

ARTICLE INFO

Keywords:
Zintl materials
GMR
spintronics
DFT
Antiferromagnetism
CMR

ABSTRACT

In the present work, the structural, electronic, magnetic, and thermodynamic properties of ternary compounds of composition XMn_2Y_2 (X = Ca, Sr; Y = P, As) are reported. The calculations are performed using the full potential augmented plane wave method (FP-APW) within the framework of density functional theory (DFT) as integrated with the WIEN2k code. The volume optimization is performed for different spin configurations to obtain the optimized unit cell structure, using the minimum energy considerations. It is found that the studied systems favor the antiferromagnetic (AFM) structure. Calculated structural parameters are in good agreement with the existing data. Based on their band structures and density of states (DOS), $CaMn_2P_2$, $SrMn_2P_2$, and $SrMn_2As_2$ have a metallic character, while $CaMn_2As_2$ is a semiconductor with a narrow band gap of 0.1161 eV on using GGA and as metallic when GGA+U is employed. The density of states diagrams show that the Mn-3*d* state contributes majorly to the valence band and the lower part of the conduction band. From stable geometries of XMn_2Y_2 compounds, it is evident that the Mn atoms are coupled antiferromagnetically in all the compounds. The large value of T_C for $CaMn_2As_2$ shows strong correspondence among the magnetic atoms. Owing to their suitable magnetic characteristics, these compounds can be used in applications such as Colossal magnetoresistance (CMR) or Giant magnetoresistance (GMR), single-molecule magnets, read heads, spin filters, spin valves, magnetic sensors, and in spintronics applications. Furthermore, temperature and pressure dependence of thermodynamic properties of these materials have been examined in the ranges (0–800 K) and (0–18 GPa), respectively.

1. Introduction

Zintl compounds possess a strong history of scientific study since their early discovery by Edward Zintl in the 1930s [1–3]. The condensed matter community has recently regained interest in these compounds due to their frequent layered transition metal structures AN_2C_2 pnictides (A = alkaline metal, N = transition metal, C = P, As, Sb, Bi) being of long-term interest in materials physics, exhibiting interesting properties, especially in magnetism and superconductivity [4]. Even though various structures are found in the Zintl phases, most of them have been studied for their remarkable magnetic properties, which are valuable for a variety of applications, such as single-molecule magnets [5] and read heads [6]. These materials are also of great technological sig-

* Corresponding author at: Department of Physics, University of Peshawar, KP, Pakistan.
E-mail address: faizanstd@uop.edu.pk (M. Faizan).

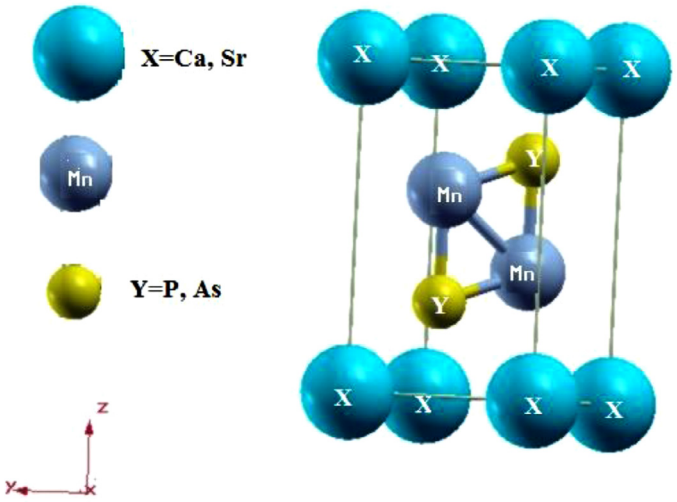

Fig. 1. Optimize structure of XMn_2Y_2, (X= Ca, Sr; Y= P, As) compounds.

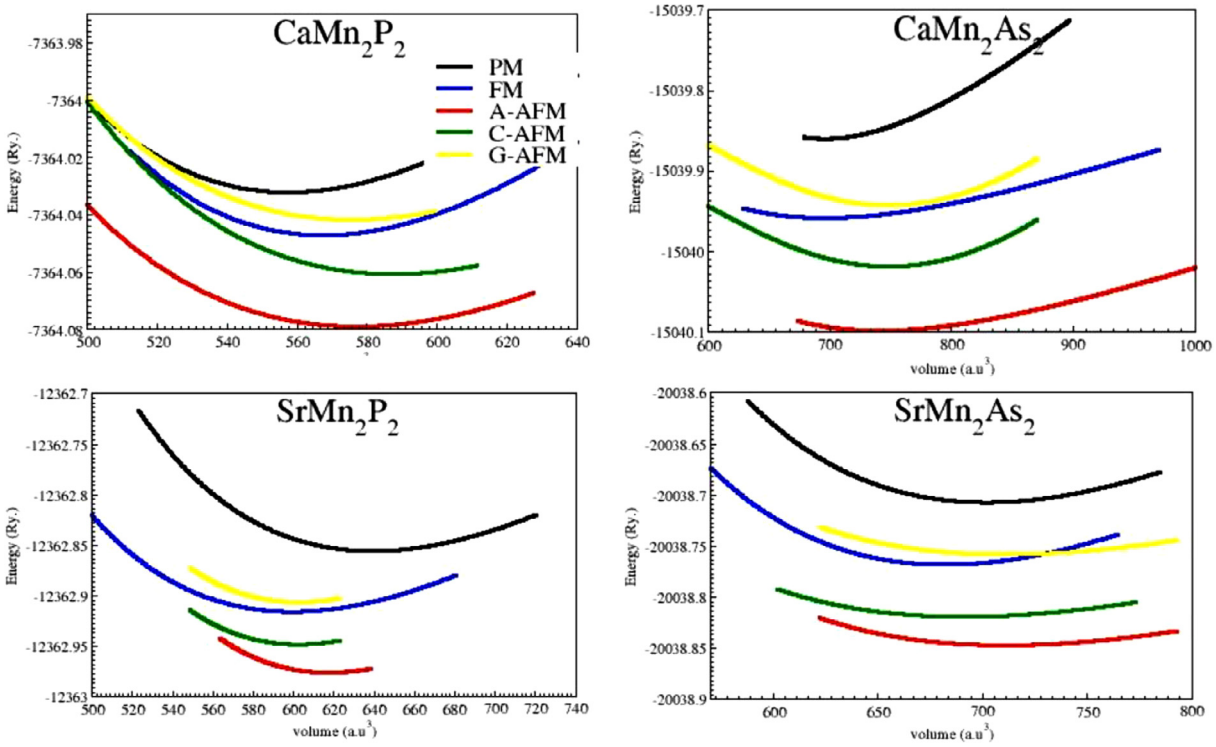

Fig. 2. Optimization plots showing energy versus volume for $CaMn_2P_2$, $CaMn_2As_2$, $SrMn_2P_2$ and $SrMn_2As_2$, respectively.

nificance as "colossal" or "giant" magneto-resistive (CMR or GMR) materials; at the same time, magneto-resistance in metallic thin films (MTF) is highly capable of altering their resistivity on the application of external magnetic field [7–9]. Several researchers have been reported work on electro-positively ternary alkaline-earth compounds of the composition AB_2X_2 (A = Ca, Sr; B = Mg, Be, Zn, Cd; X = N, P, As, Sb, Bi) [10–15], which reveal that such AB_2X_2 compounds crystallize in the trigonal $CaAl_2Si_2$ structure if the B element has a spherically symmetric d-electron distribution (d°, d^5, d^{10} configuration) in their electronic configuration [10–12]. When these conditions are fulfilled, the radius ratio r_a: r_b is also an important parameter in deciding the possibility of forming this structure, whereas the size of the X element has little influence. When the temperature T is of the order of ~200 K, the properties of these materials are essentially metallic in this regard and usually show similar structural transition and antiferromagnetic (AFM) spin-density wave state. The iron-arsenide layer plays a vital role as the conducting sheet in the growing of superconducting state in BFe_2As_2 ternary compounds [16,17]. Hence to find suitable materials for efficient superconductors, it is necessary to work on other related materials with similar structures and compositions. Such ternary compounds as follows, $SrNi_2As_2$ [18] and $BaNi_2As_2$ [19] have been found to become superconductors at Temperatures (Tc = 0.62 K) and (Tc = 0.7 K), respectively. On the other hand, $SrCo_2As_2$ [20] and $BaCo_2As_2$ [21] have similar structures with the same period metals except for Ni replaced by Co, but they have no long-range electronic correlations, contributing to superconducting and structural properties. However, the inelastic neutron scattering

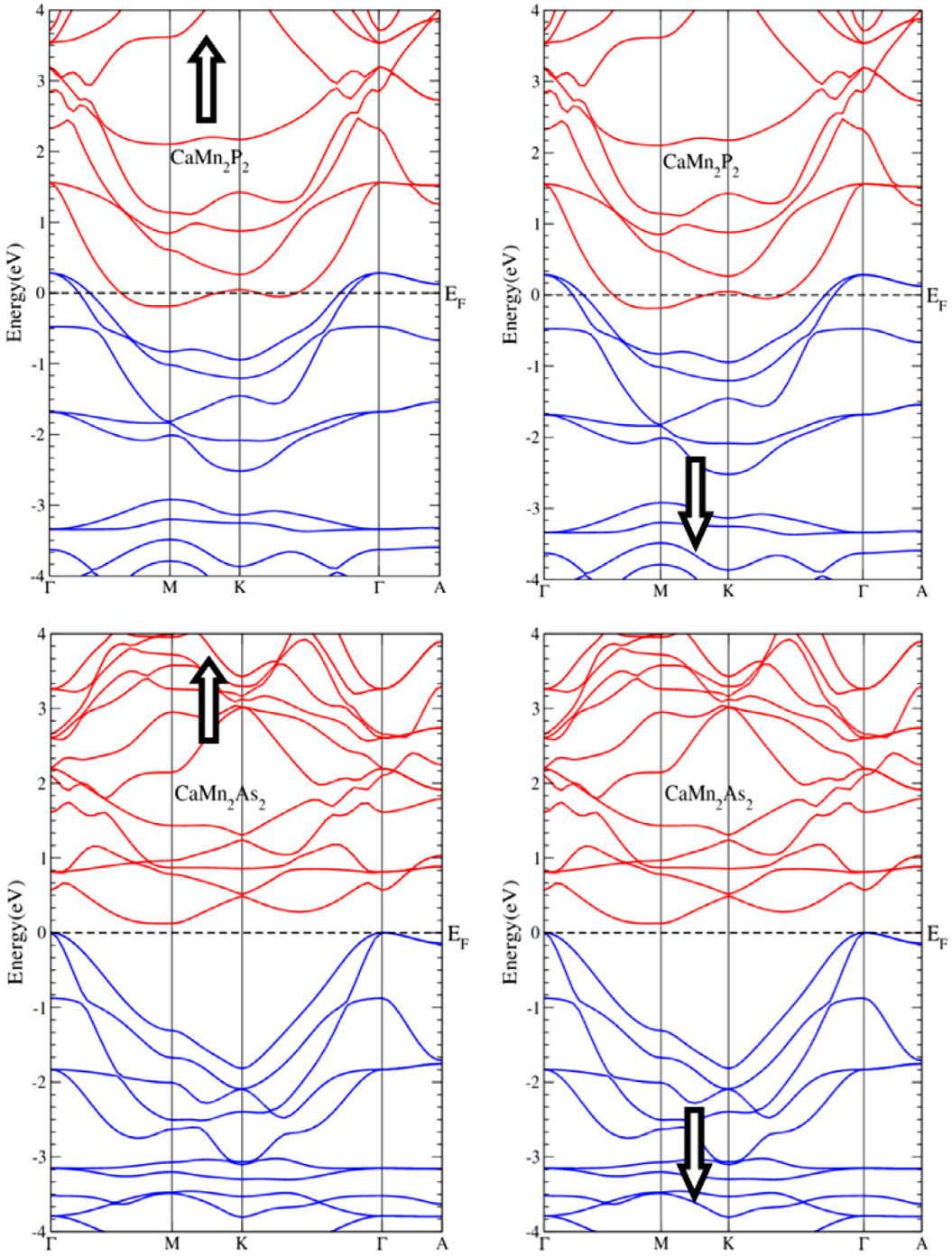

Fig. 3. Electronic band structures of $CaMn_2P_2$ and $CaMn_2As_2$ in both spin channels using GGA.

measurements show that $SrCo_2As_2$ exhibits effective AFM connection with similar patterns and shapes of wave vectors as shown by FeAs. An interesting question is that though $SrCo_2As_2$ is not a high-*Tc* superconductor [22], it shows strong ferromagnetic (FM) spin correlation, proven by NMR measurements. In FeAs, a high range of *Tc* is observed with the help of advanced NMR studies [23].

Zheng and Qin [24] studied the structural and magnetic properties of KM_2B_2 (K = Sr, Ca, M = Cr, Co, Cu, Fe, Mn, Ni, and B = P, Sb, As) hexagonal transition metal pnictides in the domain of their structure similarity, next-nearest-neighbor (N-N-N) efficient and effective antiferro-magnetic (AFM) exchange couplings using density functional theory. In both the Sr and Ca-based families, the next-nearest-neighbor (N-N-N) effective antiferromagnetic (AFM) exchange couplings achieve the highest value in the iron-based materials. While the nearest-neighbor (N-N) AFM interactions, which are mainly attributed to the direct magnetic exchange mechanism, are extremely strong in the Cr/Mn-based materials, and magnetic interactions are incredibly weak in Co / Cu / Ni-based materials.

Despite significant previous research on thorium (Th), barium (Ba), and calcium (Ca) based ternary intermetallic systems [42–44,46], as well as lanthanide-based and transition metal oxides

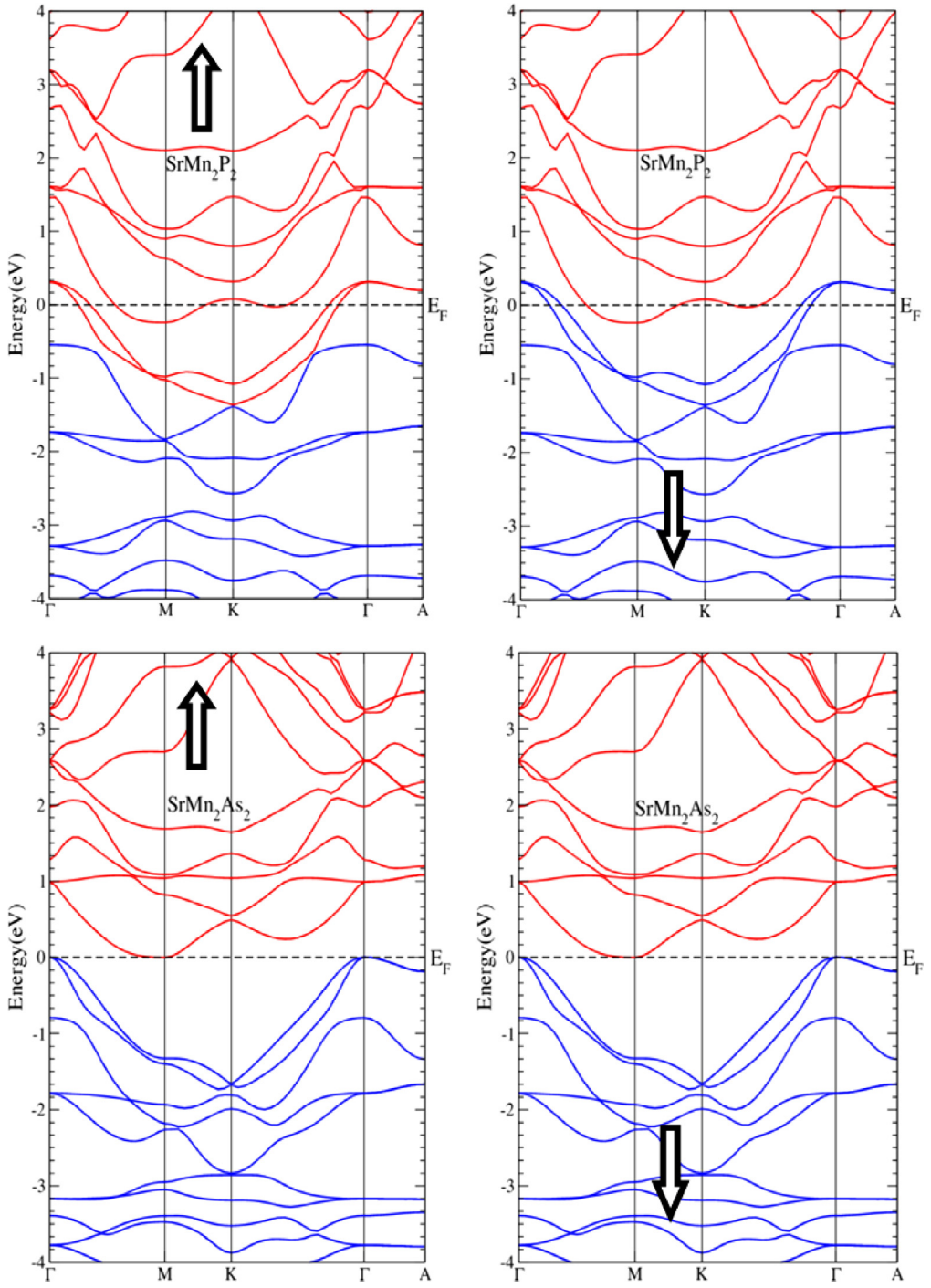

Fig. 4. Electronic band structures of $SrMn_2P_2$ and $SrMn_2As_2$ in both spin channels using GGA.

(TMO) compounds [45,47,48], possessing large magnetoresistance (M-R), they typically receive more attention due to their applications in spin filters, spin valves, magnetic sensors, and spintronic devices. But, other compounds with the same compositions like XMn_2Y_2 (X=Ca, Sr; Y=P, As) have not been studied yet.

In this work, the ternary compounds of the composition XMn_2Y_2 (X=Ca, Sr; Y=P, As) in trigonal (See Fig. 1) structure with space group $P\bar{3}m1$ (No. 164) [25] have been investigated using density functional theory. This work is important because, so far, not enough literature is available on the theoretical investigation of these compounds. Therefore, this work can provide a platform for further theoretical work and investigations of such compounds, which have high potential for spintronic applications, and further advances in magnetism and superconductivity experimental work.

2. Computational details

First-principles DFT calculations [26,27] based upon Non-magnetic (NM), AFM, and spin-polarized FP-APW method [28] within PBE-GGA [29] and GGA+U [30] framework are performed using WIEN2k code. The appropriate U_{eff} values for these compounds were adopted to be 7, 7.5 and 7.9 eV [41]. The wave functions are also increased in extent in the interstitial domain to plane waves with a cutoff of K_{max} = 7.0/RMT, which is

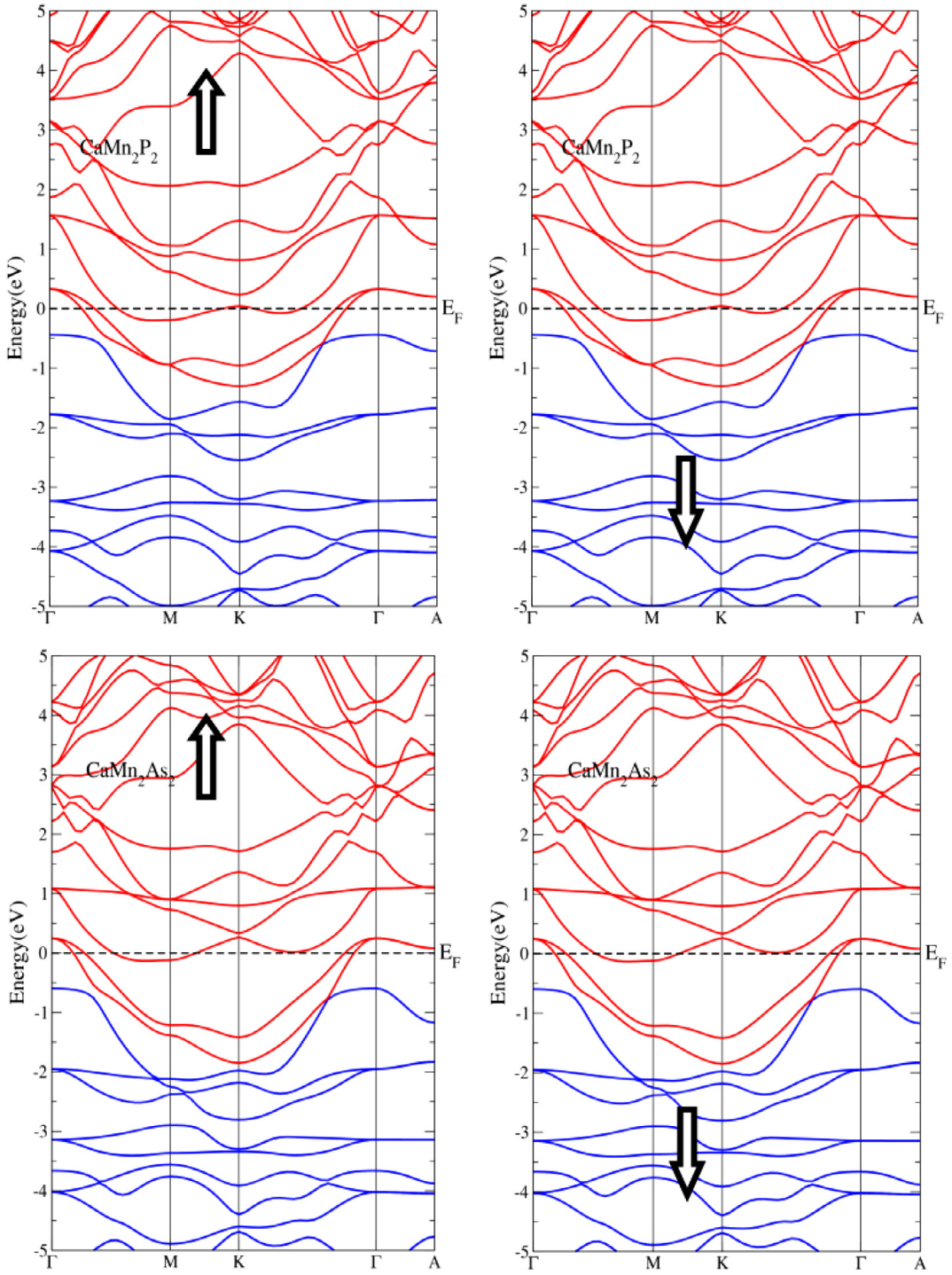

Fig. 5. Electronic band structures of $CaMn_2P_2$ and $CaMn_2As_2$ in both spin channels using GGA+U.

satisfactory in view of the common average radius of muffin-tin spheres providing us R_{MT} and K_{max} symbolizes the highest value of magnitude of K vector that accommodates all the meaningful plane waves. The separation energy between valence and core states is −6.0 Ry. The basic non-overlapping muffin-tin radii are chosen as (2.5, 2.1, 1.86) au, (2.5, 2.32, 2.06) au, (2.5, 2.14, 1.9) au, and (2.5, 2.22, 2.11) au for (Ca, Mn, P), (Ca, Mn, As), (Sr, Mn, P) and (Sr, Mn, As) elements, respectively. The 1000 k points Monkhorst–Pack mesh is used [29,31] in the Brillion zone for $CaMn_2P_2$, $CaMn_2As_2$, $SrMn_2P_2$, and $SrMn_2As_2$ compounds in the AFM phase. To get exact transport properties, a dense mesh of 5000 k points has been used. The Quasi-harmonic Debye model [32,33] has been employed to study the pressure and temperature dependence of some significant thermodynamic parameters.

3. Results and discussion

3.1. Structural properties

Structural properties of ternary compounds, XMn_2Y_2 (X=Ca, Sr; Y=P, As), are determined using PBE-functional. The optimization of analyzed configurations is done in five different spin phases, which

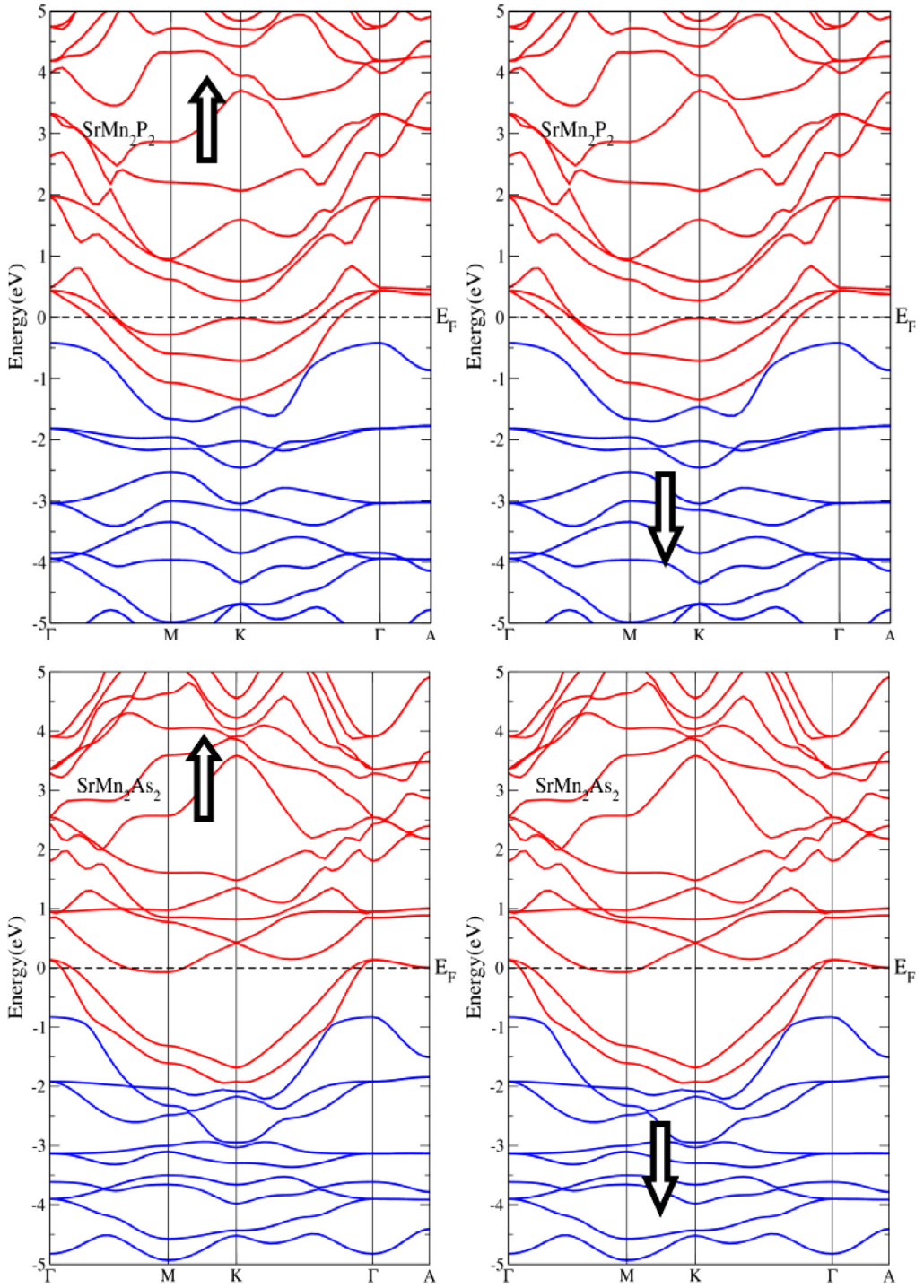

Fig. 6. Electronic band structures of $SrMn_2P_2$ and $SrMn_2As_2$ in both spin channels using GGA+U.

are of current interest because of their applications and specifically belong to antiferromagnetic (A-AFM, C-AFM, G-AFM), paramagnetic (PM), and ferro-magnetic (FM) type of materials. Fascinatingly, the considered materials become stabilized in the A-AFM phase. The antiferromagnetic phase is established by means of the energy difference $\Delta \mathbf{E=E_{FM}-E_{AFM}}$ shown in Table 1, which provides positive values for all the compounds. The present calculated structural properties (Fig. 2 and Table 1) are in good agreement with the experimental [21] and other theoretical reports [24]. An increase in the lattice constants and unit cell volume in Ca and Sr based compounds is observed on replacing P with As due to the difference in their atomic sizes, as predicted from Table 1. Values of the Bulk modulus B_0, which are obtained by volume optimization, are also listed in Table 1 for XMn_2Y_2 (X=Ca, Sr; Y=P, As). Larger value of B_0 for $SrMn_2P_2$ shows that this compound is harder and usually less compressible than the other compounds included in this study.

3.2. Electronic properties

From the electronic structure of these compounds, it is revealed that every material shows unique properties due to their different band structures. The ferromagnetic band structures of XMn_2Y_2

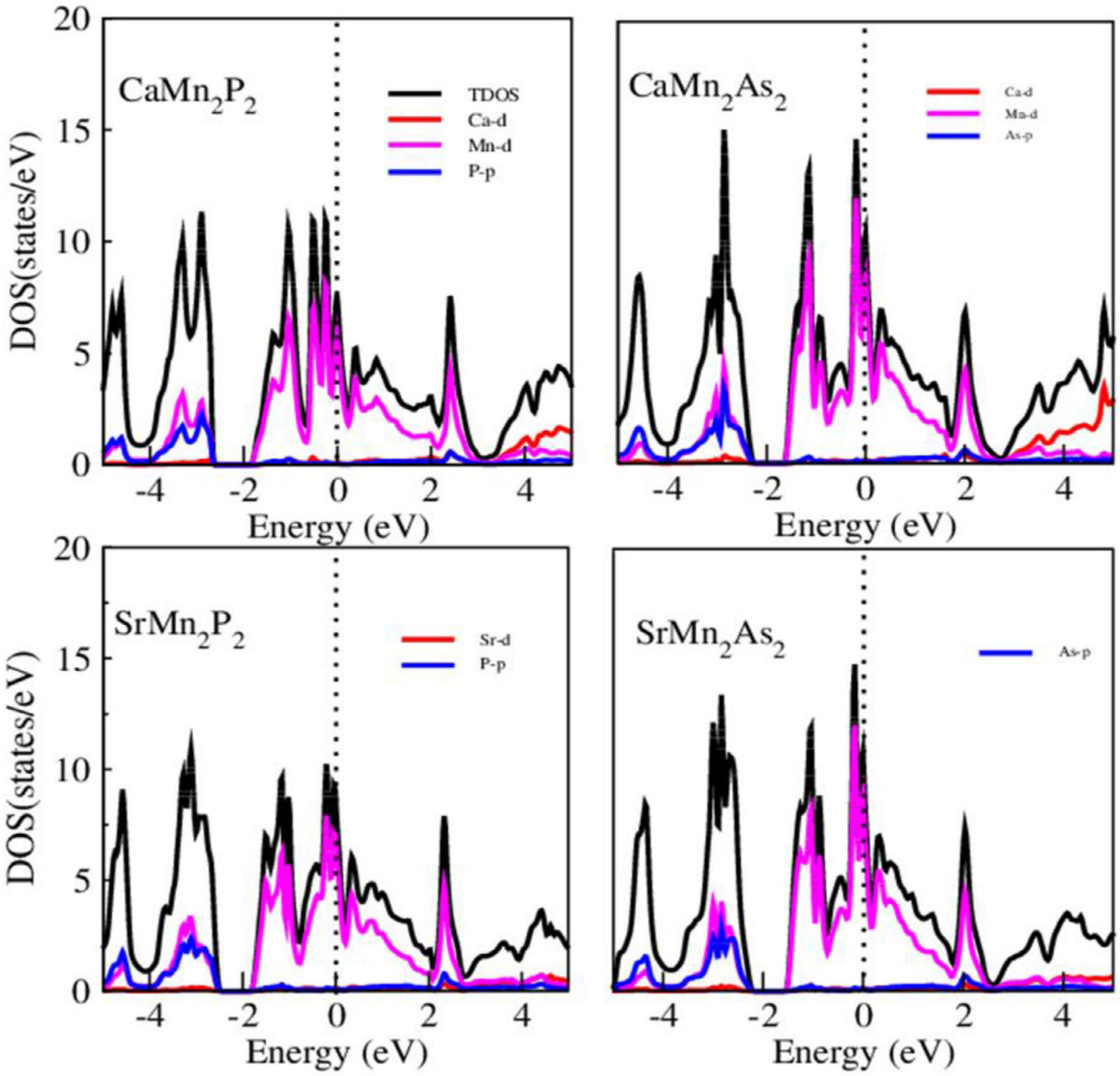

Fig. 7. DOS plots for paramagnetic ternary compounds XMn_2Y_2 (X = Ca, Sr; Y =P, As).

Table 1
Calculated lattice parameters, V_o(a.u)^3,*a* (Å), B (GPa), and E_0 (Ry) for antiferromagnetic ternary compounds along with experimental and other theoretical results.

	Vo	a	c	B(GPa)	E0 (Ry)				T_C(K)
					A-AFM	C-AFM	G-AFM	$\Delta E=E_{FM}-E_{AFM}$	
$CaMn_2P_2$	579.80	4.10	6.82	92.39	−7364.08	−7364.06	−7364.04	0.01	525.60
Exp:		4.10(a)	6.84(a)						
Theory		4.11(b)	6.80(b)						
$CaMn_2As_2$	750.04	4.25	7.1	79.59	−15040.01	−15039.05	−15039.83	0.11	5781.6
Exp:		4.24(a)	7.03(a)						
Theory		4.26(b)	7.00(b)						
$SrMn_2P_2$	602.15	4.14	7.18	173.65	−12362.98	−12362.93	−12362.92	0.03	1576.8
Exp:		4.17(a)	7.13(a)						
Theory		—-	—-						
$SrMn_2As_2$	710.88	4.2	7.19	54.20	−20038.85	−20038.82	−20038.74	0.01	525.60
Exp:		4.31(a)’	7.31(a)						
Theory		—-	—-						

[a]Ref: [21],[b]Ref: [24]

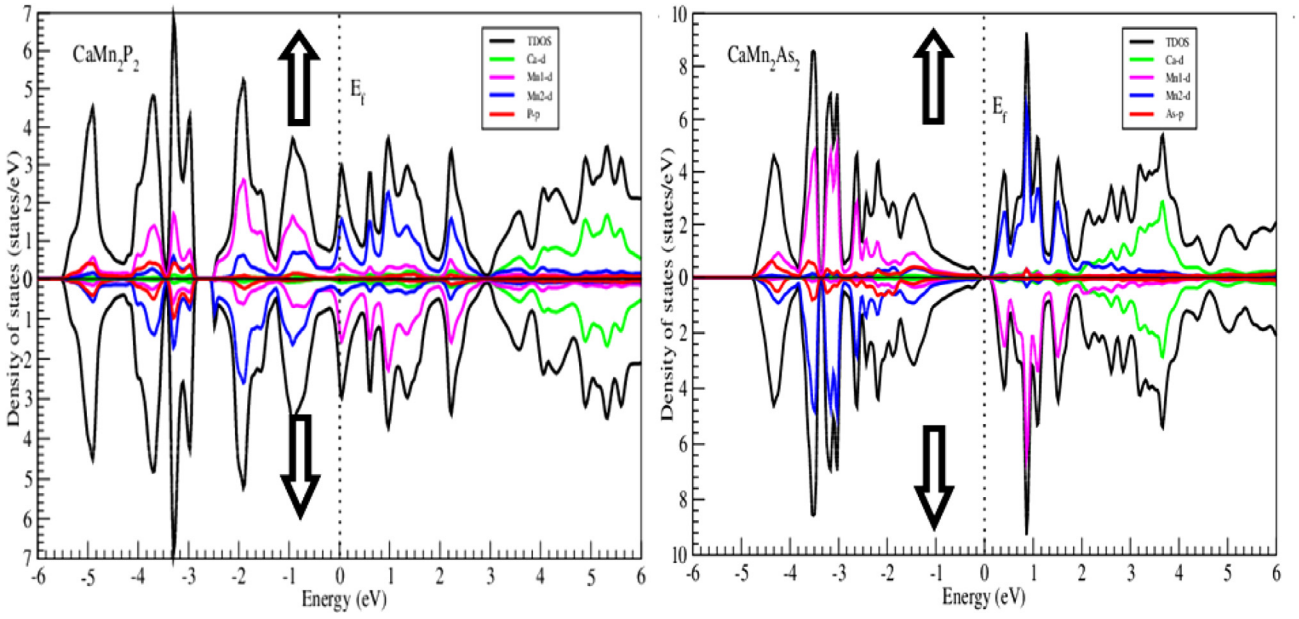

Fig. 8. GGA+U calculated DOS plots for $CaMn_2P_2$ and $CaMn_2As_2$ in Antiferromagnetic phase in both spin types.

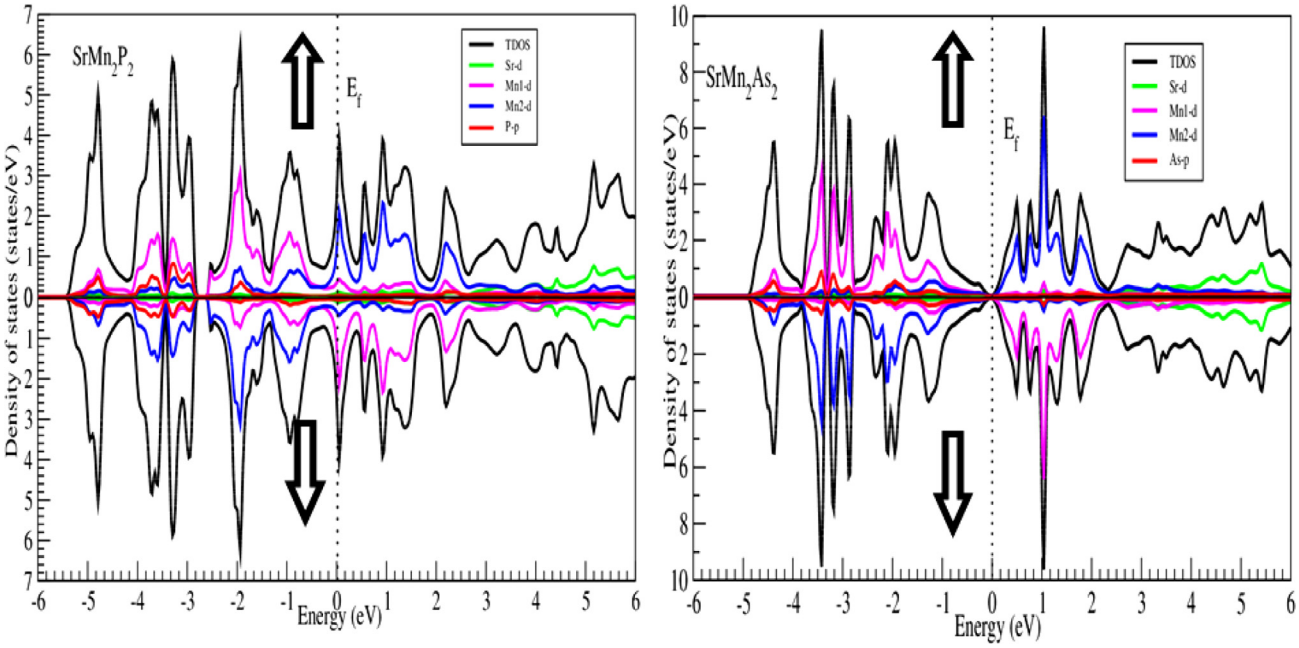

Fig. 9. GGA+U calculated DOS plots for $SrMn_2P_2$ and $SrMn_2As_2$ in Antiferromagnetic phase in both spin types.

(X=Ca, Sr; Y=P, As) by employing the two approximations (viz. PBE-GGA and GGA+U) with spin-up and spin-down channels along the high symmetry directions in the first Brillouin zone are illustrated in Figs. 3, 4, and Figs. 5, 6, respectively. It is established from Figs. 3–6 that $CaMn_2P_2$, $SrMn_2P_2$, and $SrMn_2As_2$ are metallic in nature with overlapping valence and conduction bands; while $CaMn_2As_2$ is a semiconductor with a small narrow band gap of 0.1161 eV with GGA (Fig. 3) and shows metallic character on using GGA+U (Fig. 5). To understand the electronic origin of band structures, total and partial densities of states (DOS) are also calculated for all the four compounds, and relevant DOS plots are displayed in Figs. 7–9. Along with the stable AFM phase, the PM phase has also been investigated in the present work due to the possibility that these materials can exist in the PM phase above Neel temperature. From the projected density of states (PDOS), as shown in Fig. 7, one can see that Ca-*d*, Sr-*d*, and Mn-*d* states and P-*p*, As-*p* states mainly contribute to the total density of states (TDOS) in the PM phase. The DOS close to the Fermi level (E_F) of the PM phase shows the metallic nature of the studied materials, and they may be unstable mainly because of the Stoner argument [34–36], and possibly another phase is achieved on permitting spin polarization to be included in the calculations.

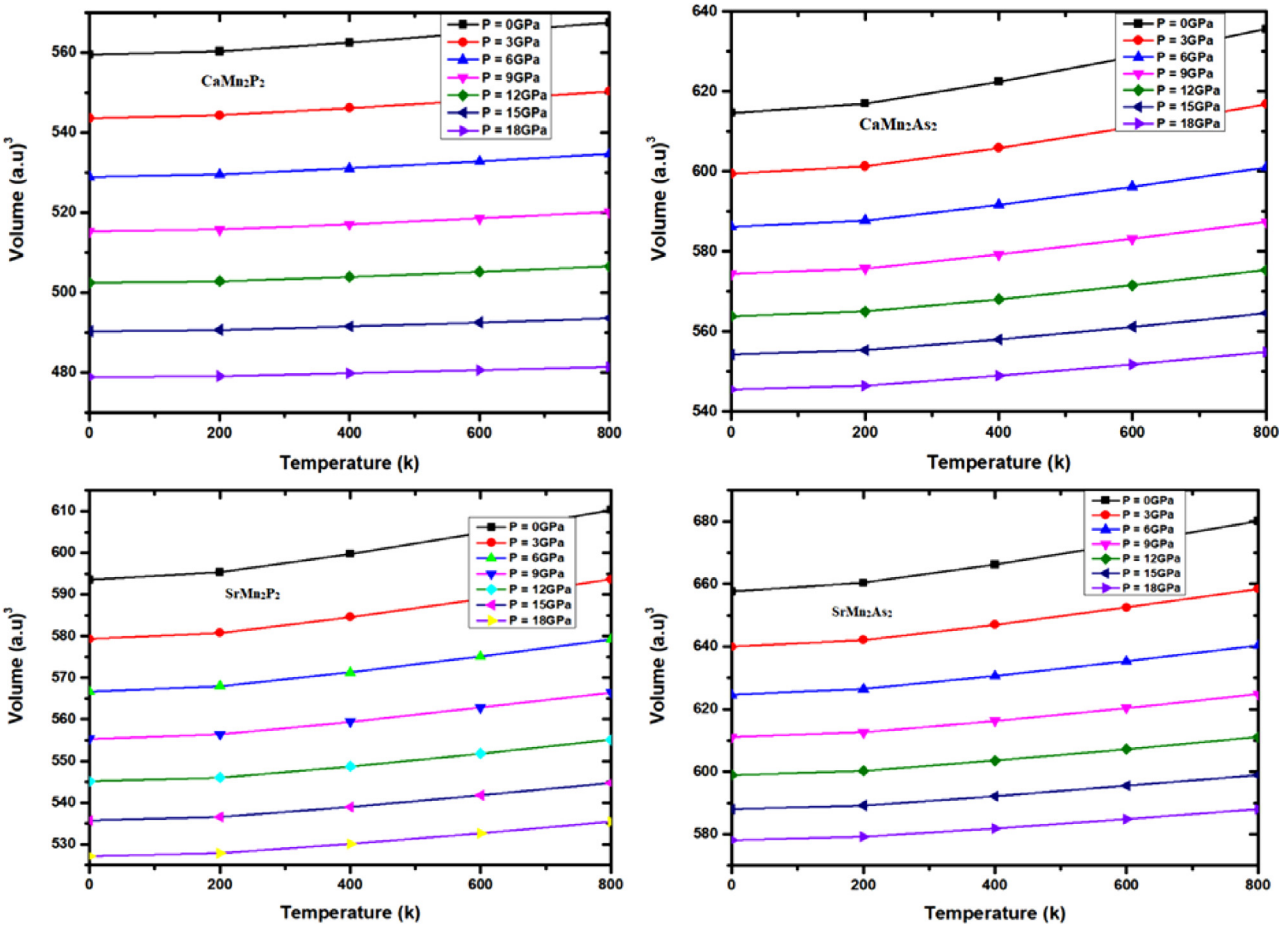

Fig. 10. Variation of unit cell volume with temperature and pressure for XMn_2Y_2.

Further, the DOS of $CaMn_2P_2$, $CaMn_2As_2$, $SrMn_2P_2$, and $SrMn_2As_2$ are also calculated in AFM phase, as shown in Figs. 8 and 9 with GGA+U method. DOS analysis helps to see how much each state contributes to the conduction and valence bands, respectively. The major contributions are made by *d* (Ca, Mn_1, Mn_2), *p* (P), and *d* (Ca, Mn_1, Mn_2), and *p* (As) states for $CaMn_2P_2$ and $CaMn_2As_2$, respectively, in both spin-types. Interestingly, Mn-3d in $CaMn_2As_2$ and $SrMn_2As_2$ are moved toward the VB in GGA+U approximation, indicating that GGA+U is more appropriate for accurately describing the exchange and correlation interactions in the given systems.

The *p* states of anions (P, As) and cation (Ca-*d*) is positioned in Valence Band (VB) and Conduction Band (CB) mainly for both spin-types. For spin-up, Mn_1-d state is switched oppositely to that Mn_2-d in spin-down channel, it means that both Mn atoms are well adjusted antiferromagnetically. In these compounds, *p*-*d* hybridization is indicated between *p* (P, As) and *d* (Mn) orbitals. Hybridization for AFM is vital for unfilled *d*-band based upon (direct or double) exchange. These AFM states show that direct exchange couplings occur between two nearest-neighbor (NN) Mn atoms. The DOS plot of $CaMn_2P_2$ shows metallic character, and similarly, for $CaMn_2As_2$, it shows very narrow band gap of 0.1161 eV at the E_F for both spin types with GGA and metallic with GGA+U as apparent from Figs. 7 and 8.

For $SrMn_2P_2$ and $SrMn_2As_2$, the DOS schematic plots are shown in Fig. 9. The major contributions to total DOS are from *d* (Sr, Mn_1, Mn_2), *p* (P) and *d* (Sr, Mn_1, Mn_2), *p* (As) states for $SrMn_2P_2$ and $SrMn_2As_2$, respectively, in both spin styles. Similarly, cation (Sr) and anions (P, As) contribute majorly. In spin-up and down configurations, Mn_1-*d* and Mn_2-*d* contribute oppositely to each other in both compounds. The starting and ending of the density of states for these cases are the same, suggesting that in AFM case both the magnetic moments are zero. The DOS of the compound $SrMn_2P_2$ shows its metallic nature, and $SrMn_2As_2$ shows semimetal character across the E_f in both spins states (Fig. 9).

3.3. Magnetic properties

To describe the magnetic nature of these Zintl compounds, we analyzed ferromagnetic and antiferromagnetic configurations by employing the GGA and GGA+*U* schemes. The basic source of strong magnetization in these compounds is the unoccupied Mn-3*d* orbital. Furthermore, the Mn-3*d* state splits into partially filled sub-*d* states. This initiates ferromagnetism in the above-stated compounds. The magnetic moments per unit cell in ferromagnetic and antiferromagnetic configurations are listed in Tables 2 and 3, respectively. In both GGA and GGA+U schemes, it is observed that Mn ions provide the most contribution to the total magnetic moment as compared to the interstitial regions and individual atoms. In case of GGA+U calculations, by varying the U_{eff} values from 7 to 7.9 eV for XMn_2Y_2 (X=Ca, Sr; Y=P, As), we note an increase in the total magnetic moment due to the increasing partial magnetic moments of Mn, X and Y atoms. The negative values of the magnetic moments of Y atoms indicate that they exhibit an anti-parallel alignment with Mn to reduce the net magnetic moments, while the positive values of the magnetic moment of X atoms show that they are aligned parallel to the Mn atom.

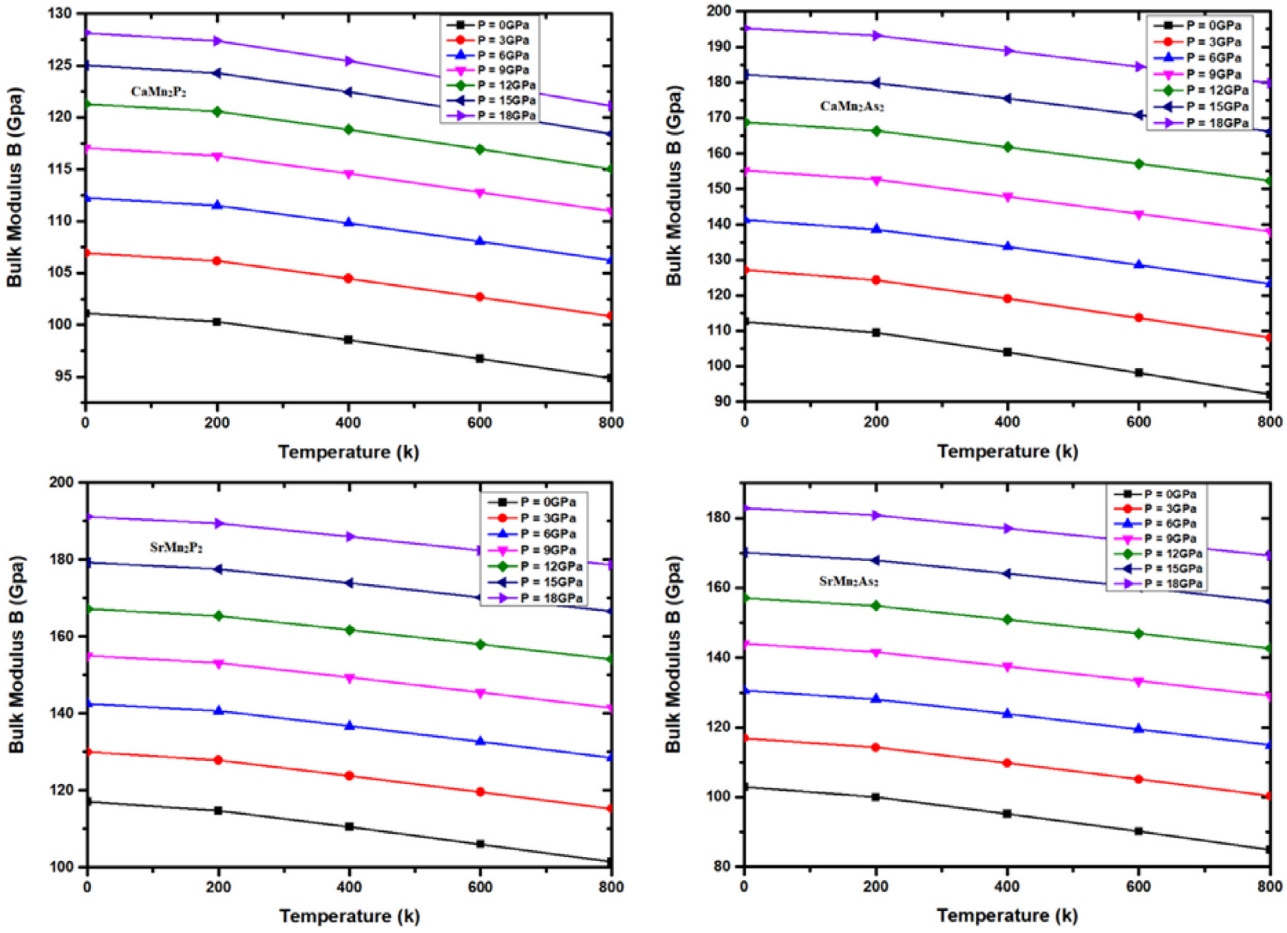

Fig. 11. Bulks modulus (B) versus temperature and pressure for XMn_2Y_2.

Table 2
Magnetic moments of the interstitial domain (m^{inst}), individual atoms ($m^{Ca/Sr}$, m^{Mn1},$m^{Mn2,}$ $m^{P/As}$) and entire unit cell (m_c) for ternary compounds XMn_2Y_2 (X= Ca, Sr; Y = P, As) for spin Ferro configuration using GGA and GGA+U.

Magnetic Moments	$CaMn_2P_2$	$CaMn_2As_2$	$SrMn_2P_2$	$SrMn_2As_2$
GGA				
m_c	3.5	5.1	4.2	5.7
m^{inst}	0.077	0.172	0.204	0.2361
$m^{Ca/Sr}$	0.0007	-0.0007	0.005	0.009
m^{Mn}	1.81	2.59	2.0854	2.87381
$m^{P/As}$	-0.1070	-0.0970	-0.0791	-0.12124
GGA+U				
U_{eff}=7 eV				
m_c	4.7	5.12	4.22	5.8
m^{inst}	0.871	0.708	0.745	0.718
$m^{Ca/Sr}$	0.0858	0.0546	0.0601	0.0377
m^{Mn}	2.15	2.3	1.53	2.88
$m^{P/As}$	-0.0247	-0.0081	-0.0798	-0.0168
U_{eff}=7.5 eV				
(Ueff=7 eV)				
m_c	4.8	5.13	4.3	5.82
m^{inst}	0.873	0.697	0.761	0.704
$m^{Ca/Sr}$	0.0858	0.0531	0.0618	0.0337
m^{Mn}	2.16	2.32	1.55	2.9
$m^{P/As}$	-0.0249	-0.0109	-0.0774	-0.0083
U_{eff}=7.9 eV				
m_c	4.82	5.15	4.4	5.83
m^{inst}	0.874	0.688	0.835	0.693
$m^{Ca/Sr}$	0.0855	0.0519	0.0628	0.0327
m^{Mn}	2.18	4.6180	2.1	2.92
$m^{P/As}$	-0.0248	-0.0139	-0.0579	-0.0106

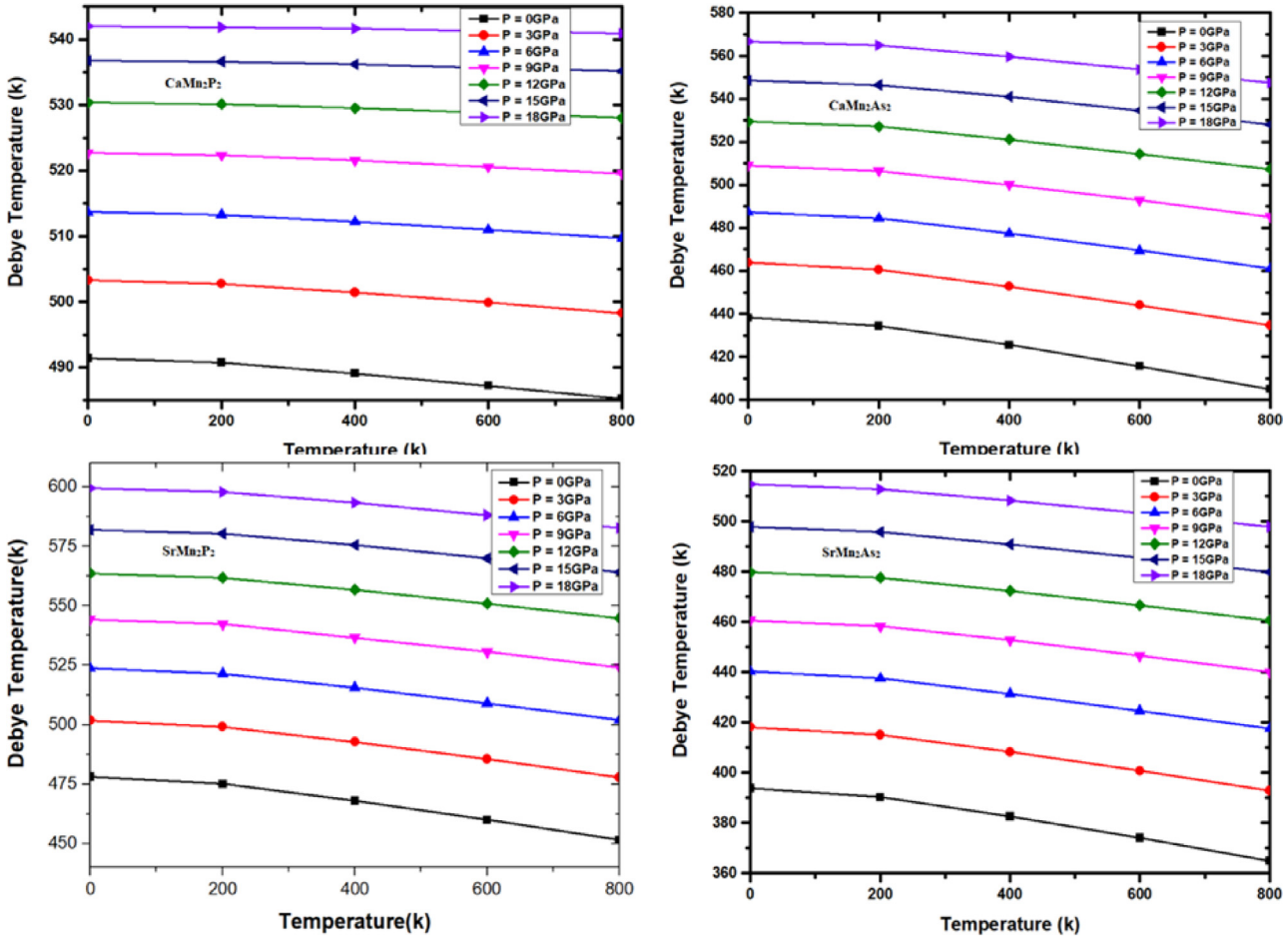

Fig. 12. Debye temperature (θ_D) versus temperature and pressure for XMn_2Y_2.

Table 3
Magnetic moments of the interstitial domain (m^{inst}), individual atoms ($m^{Ca/Sr}$, m^{Mn1},$m^{Mn2,}$ $m^{P2/As2}$) plus total cell for XMn_2Y_2 (X= Ca, Sr; Y = P, As) for spin Antiferromagnetic configuration using GGA+U.

Compound	m^{Inst}	$m^{Ca/Sr}$	m^{Mn1}	m^{Mn2}	$m^{P1/As1}$	$m^{P2/As2}$	m_c
$CaMn_2P_2$	0.0002	0.0000	2.6485	−2.6479	−0.0201	0.0201	0.0008
$CaMn_2As_2$	0.0000	0.0000	3.3291	−3.3291	−0.0101	0.0101	0.0000
$SrMn_2P_2$	−0.0003	−0.0000	2.6405	−2.6415	0.0340	−0.0340	−0.0014
$SrMn_2As_2$	0.0000	0.0000	3.6678	−3.6678	0.0063	−0.0063	0.0000

From the analysis of the GGA and GGA+U approximations in ferromagnetic configuration, it is observed that the magnetic moment value shows an increasing tendency when the Hubbard parameter is increased. The total cell magnetic moments, $\mathbf{m_c}$, for each compound and individual atomic magnetic moments in antiferromagnetic configuration with GGA+U are given in Table 3. As can be seen from Table 3 that in all XMn_2Y_2 compounds, both Mn atoms are well coupled antiferromagnetically. We have also computed the Curie temperature (T_C) of XMn_2Y_2 (X=Ca, Sr; Y=P, As) compounds by the analytical method [37,38] and compared it with previous work [39] in Table 1. The Larger value of T_C for $CaMn_2As_2$ shows the substantial interaction among the magnetic atoms in this compound as compared to other compounds investigated in the present research.

3.4. Thermodynamic properties

The attractive thermodynamic properties of these compounds have been calculated by means of quasi-harmonic Debye model [32,33]. For pressure and temperature variations in the ranges 0 to 18 GPa and 0 to 800 K, respectively, the corresponding deviation of volume (V), specific heat at constant volume (C_v), Bulks modulus (B), thermal expansion (α), and Debye temperature (θ_D) are determined for XMn_2Y_2. In Fig. 10, the volume of the unit cell is plotted against temperature and pressure. It can be observed from these plots that volume is directly proportional to the temperature at a certain pressure. Conversely, volume is inversely proportional to the change in pressure at a certain temperature. Usually, this process is frequently used in solids because with larger pressure compression occurs, and larger increase in temperature expansion occurs in solids. From Fig. 11, it is observed that the bulk moduli of all the compounds investigated in the present research show opposite trend as compared to volume deviation. The bulk modulus shows a direct relationship with the pressure and inverse relation with temperature in all the compounds. The argument for this rise and fall in B with pressure and temperature is due to the fact that when temperature decreases, the hardness increases due to reduction in cell dimensions and volume, and similarly, the hardness

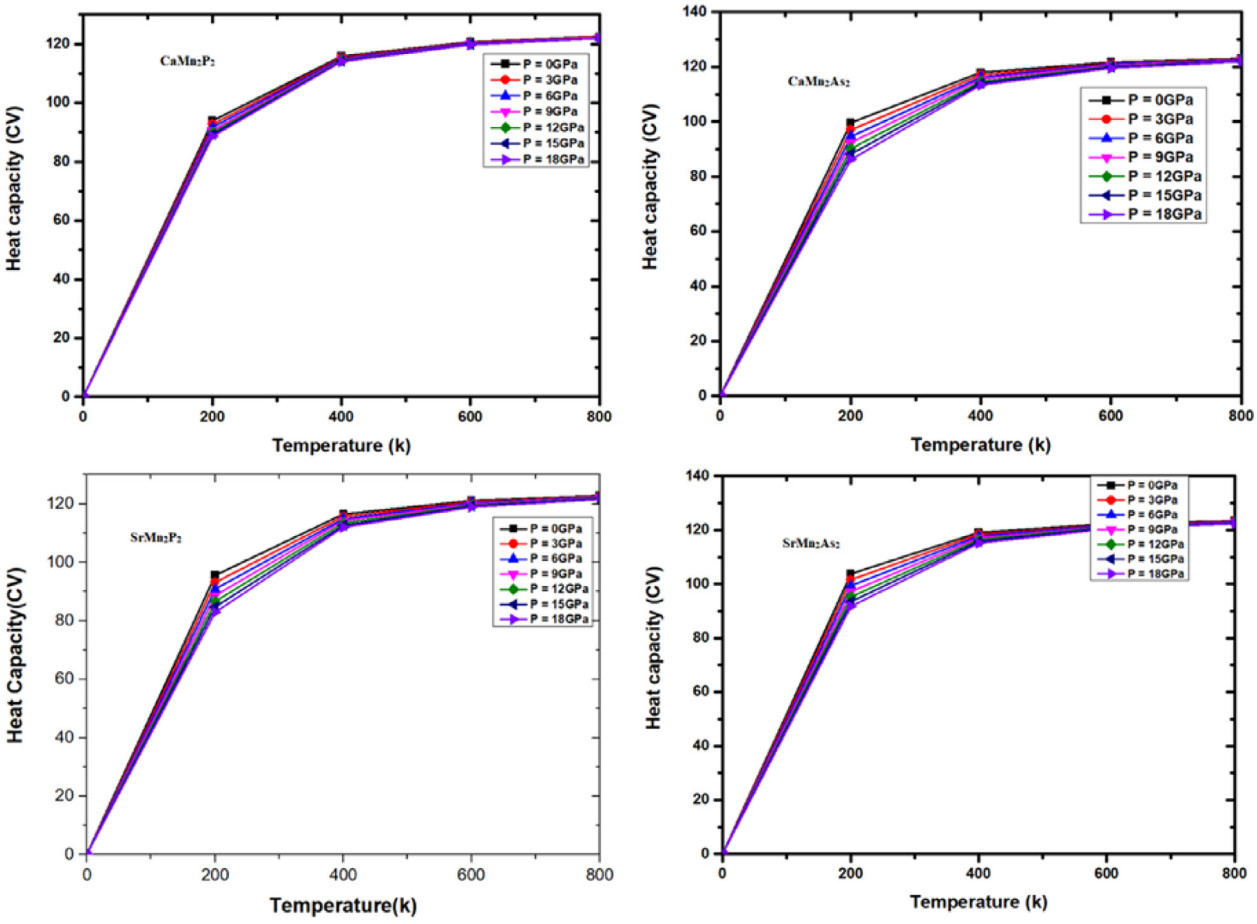

Fig. 13. Nature of specific heat at constant volume (Cv) versus temperature and pressure for XMn_2Y_2.

increases with an increase in pressure. In both cases, bulk moduli increase, whereas increasing temperature causes an increase in inter-atomic distance and volume of the unit cell. Thus, pressure has an inverse relation with temperature. The value of B calculated from optimization closely agrees with the thermodynamic data. Finally, we have shown the variation of Debye temperature (θ_D) with temperature for XMn_2Y_2 in Fig. 12. The temperature above which a crystal displays classical behavior is called Debye temperature (θ_D). Debye temperature describes the precise arrangement of material properties like its thermal expansion and specific heat capacity. It is seen that θ_D decreases with increasing temperature and pressure. The calculated value of Debye temperature at 300 K and 0 GPa is 564 K.

In Fig. 13, the dependence of specific heat at invariant volume (C_V) on temperature and pressure is shown for these compounds. The phase transition or lattice vibrations are determined by C_V, and it increases the motion of the molecules. It may be observed from Fig. 13 that C_V is growing fast from 0 to 110 K for all the compounds, while it increases in ascending order from 0 GPa to 18 GPa, and for higher than 120 K temperature, a slow increase is observed in C_V, further, it becomes constant at about 500 K and reaches the Dulong-Petit limit [40]. The calculated value of C_V for $CaMn_2P_2$, $CaMn_2As_2$, $SrMn_2P_2$, and $SrMn_2As_2$ at 200 K and 0 GPa are 86, 98, 98, and 102 J mol^{-1} K^{-1}. The computed values of C_V under ambient conditions can provide useful information for experimental work. The behavior of thermal expansion coefficient (α) with changes in pressure and temperature is shown in Fig. 14. It is seen that 'α' increases rapidly up to 400 K, above which a slow rise in 'α' is observed. This is due to saturation of 'α' above 400 K. The thermal expansion coefficient has an inverse relation with pressure; with rising pressure, 'α' decreases rapidly, as shown in Fig. 14. The value of 'α' for $CaMn_2P_2$, $CaMn_2As_2$, $SrMn_2P_2$, and $SrMn_2As_2$ under 200 K and 0 GPa pressure was found to be 1.75×10^{-5} K^{-1}, 3.75×10^{-5} K^{-1}, 3.25×10^{-5} K^{-1}, and 3.8×10^{-5} K^{-1}, respectively.

4. Summary

In summary, we have investigated the structural, electronic, magnetic, and thermodynamic properties of XMn_2Y_2 compounds using first-principles calculations. From energy considerations for different phases, it has been established that in all XMn_2Y_2 compounds, both Mn atoms are well coupled antiferromagnetically in A-AFM phases. From the demonstration of projected density of states (PDOS) diagrams, a well-defined hybridization occurs between Mn-3*d* and P-*p* states and similarly for Mn-3d and As-*p* states. We have found that $CaMn_2P_2$, $SrMn_2P_2$, and $SrMn_2As_2$ compounds possess metallic character, whereas $CaMn_2As_2$ is a semiconductor with a narrow band gap of 0.1161 eV with GGA and is metallic with GGA+U. Larger value of T_C for $CaMn_2As_2$ shows the presence of strong interaction among the magnetic atoms as compared to other compounds. Further, the thermodynamic parameters of these compounds indicate strong pressure and temperature dependence. Owing to their promising magnetic characteristics, these compounds are suitable for application in spin valves, magnetic sensors, and spintronic devices.

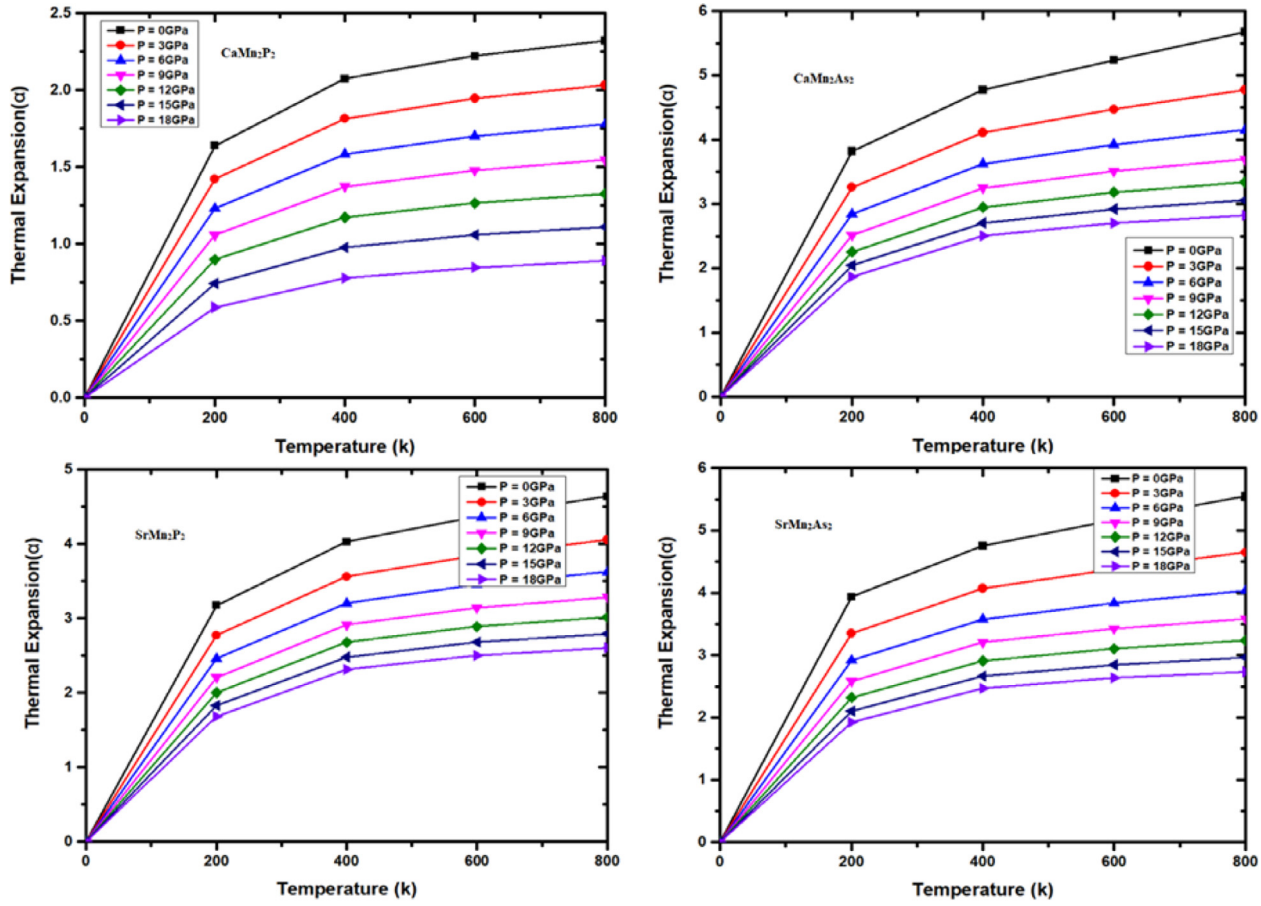

Fig. 14. Thermal expansion (α) with respect to temperature and pressure for XMn_2Y_2.

Declaration of Competing Interest

The authors declare that they have no known conflicts of interest associated with this article.

CRediT authorship contribution statement

Zeshan Zada: Data curation, Investigation, Methodology, Writing – original draft. **Rifaqat Zada:** Investigation, Software, Methodology, Resources. **Abdul Ahad Khan:** Investigation, Methodology, Resources, Writing – review & editing. **Muhammad Saqib:** Investigation, Project administration. **Muhammad Fazal Ur Rehman:** Formal analysis, Resources, Investigation, Writing – review & editing. **Muhammad Ismail:** Investigation, Project administration, Supervision. **Neeraj Kulhari:** Formal analysis, Methodology, Investigation, Writing – original draft. **Krishna Swaroop Sharma:** Investigation, Project administration, Supervision. **Muhammad Ismail:** Investigation, Software, Methodology, Writing – review & editing. **Xingchen Shen:** Formal analysis, Investigation, Writing – review & editing. **Muhammad Faizan:** Conceptualization, Formal analysis, Software, Investigation, Methodology, Writing – original draft, Writing – review & editing.

Data availability

No data was used for the research described in the article.

References

[1] H. Schaefer, On the Problem of Polar Intermetallic Compounds: The Stimulation of E. Zintl's Work for the Modern Chemistry of Intermetallics, Annu. Rev. Mater. Sci. 15 (1985) 1–41.

[2] S.M. Kauzlarich, Chemistry, Structure, and Bonding of Zintl Phases and Ions, VCH Publishers, 1996.

[3] H. Schäfer, B. Eisenmann, W. Müller, Zintl phases: transitions between metallic and ionic bonding, Angew. Chem. Int. Ed. 12 (1973) 694–712 English, doi:10.1002/anie.197306941.

[4] E. Morosan, H. Zandbergen, B. Dennis, J. Bos, Y. Onose, T. Klimczuk, A. Ramirez, N. Ong, R. Cava, Superconductivity in Cu_xTiSe_2, Nat. Phys. 2 (2006) 544.

[5] S. Bobev, J.D. Thompson, J.L. Sarrao, M.M. Olmstead, H. Hope, S.M. Kauzlarich, Probing the limits of the zintl concept: structure and bonding in rare-earth and alkaline-earth zinc-antimonides $Yb_9Zn_{4+x}Sb_9$ and $Ca_9Zn_{4.5}Sb_9$, Inorg. Chem. 43 (2004) 5044–5052, doi:10.1021/ic049836j.

[6] J.A. Brug, T.C. Anthony, J.H. Nickel, Magnetic recording head materials, MRS Bull. 21 (1996) 23–27, doi:10.1557/S0883769400036320.

[7] Z. Zada, A. Laref, G. Murtaza, A. Zeb, A. Yar, First-principles calculations of electronic and magnetic properties of XMn_2Y_2 (X= Ca, Sr; Y= Sb, Bi) compounds, Int. J.Mod. Phys. B 33 (2019) 1950199, doi:10.1142/S0217979219501996.

[8] Z. Zada, H. Ullah, R. Zada, S. Zada, A. Laref, S. Azam, S. Azam, A.A. Khan, M. Irfan, Structure stability, half metallic ferromagnetism, magneto-electronic and thermoelectric properties of new zintl XCr_2Bi_2 (X= Ca, Sr) compounds for spintronic and renewable energy applications, Phys. B Condens. Matter 607 (2021) 412866, doi:10.1016/j.physb.2021.412866.

[9] Z. Zada, H. Ullah, R. Bibi, S. Zada, A. Mahmood, Electronic band profiles and magneto-electronic properties of ternary XCu_2P_2 (X= Ca, Sr) compounds: insight from ab initio calculations, Z. Naturforsch. A 75 (2020) 543–549, doi:10.1515/zna-2020-0053.

[10] D.C. Johnston, The puzzle of high temperature superconductivity in layered iron pnictides and chalcogenides, Adv. Phys. 59 (2010) 803–1061, doi:10.1080/00018732.2010.513480.

[11] G.R. Stewart, Superconductivity in iron compounds, Rev. Mod. Phys. 83 (2011) 1589, doi:10.1103/RevModPhys.83.1589.

[12] D.J. Scalapino, A common thread: the pairing interaction for unconventional superconductors, Rev. Mod. Phys. 84 (2012) 1383, doi:10.1103/RevModPhys.84.1383.

[13] A.A. Khan, M. Yaseen, A. Laref, G. Murtaza, Impact of anion replacement on the optoelectronic and thermoelectric properties of CaMg2X2, X=(N, P, As, Sb, Bi) compounds, Phys. B Condens. Matter 541 (2018) 24–31, doi:10.1016/j.physb.2018.04.034.

[14] A.A. Khan, A.U. Rehman, A. Laref, M. Yousaf, G. Murtaza, Structural, optoelec-

tronic and thermoelectric properties of ternary $CaBe_2X_2$ (X= N, P, As, Sb, Bi) compounds, Z. Naturforsch. A 73 (2018) 965–973, doi:10.1515/zna-2018-0204.
[15] G. Murtaza, A.A. Khan, M. Yaseen, A. Laref, N. Ullah, I. ur Rahman, The effect of replacing pnictogen elements on the physical properties SrMg2(, P, As, Sb, Bi) zintl compounds, Chin. Phys. B 27 (2018) 047102, doi:10.1088/1674-1056/27/4/047102.
[16] R.M. Fernandes, A.V. Chubukov, J. Schmalian, What drives nematic order in iron-based superconductors, Nat. Phys. 10 (2014) 97–104, doi:10.1038/nphys2877.
[17] H. Hosono, K. Kuroki, Iron-based superconductors: Current status of materials and pairing mechanism, Phys. C Supercond. Appl. 514 (2015) 399–422, doi:10.1016/j.physc.2015.02.020.
[18] E.D. Bauer, F. Ronning, B.L. Scott, J.D. Thompson, Superconductivity in $SrNi_2As_2$ single crystals, Phys. Rev. B 78 (2008) 172504, doi:10.1103/PhysRevB.78.172504.
[19] F. Ronning, N. Kurita, E.D. Bauer, B.L. Scott, T. Park, T. Klimczuk, R. Movshovich, J.D Thompson, The first order phase transition and superconductivity in $BaNi_2As_2$ single crystals, J. Phys. Condens. Matter 20 (2008) 342203, doi:10.1088/0953-8984/20/34/342203.
[20] A. Pandey, D.G. Quirinale, W. Jayasekara, A. Sapkota, M.G. Kim, R.S. Dhaka, Y. Lee, T.W. Heitmann, P.W. Stephens, V. Ogloblichev, A. Kreyssig, Crystallographic, electronic, thermal, and magnetic properties of single-crystal $SrCo_2As_2$, Phys. Rev. B 88 (2013) 014526, doi:10.1103/PhysRevB.88.014526.
[21] A.S. Sefat, D.J. Singh, R. Jin, M.A. McGuire, B.C. Sales, D. Mandrus, Renormalized behavior and proximity of $BaCo_2As_2$ to a magnetic quantum critical point, Phys. Rev. B 79 (2009) 024512, doi:10.1103/PhysRevB.79.024512.
[22] W. Jayasekara, Y. Lee, A. Pandey, G.S. Tucker, A. Sapkota, J. Lamsal, S. Calder, D.L. Abernathy, J.L. Niedziela, B.N. Harmon, A. Kreyssig, Stripe antiferromagnetic spin fluctuations in $SrCo_2As_2$, Phys. Rev. Lett. 111 (2013) 157001, doi:10.1103/PhysRevLett.111.157001.
[23] P. Wiecki, B. Roy, D.C. Johnston, S.L. Bud'ko, P.C. Canfield, Y. Furukawa, Competing magnetic fluctuations in iron pnictide superconductors: role of ferromagnetic spin correlations revealed by NMR, Phys. Rev. Lett. 115 (2015) 137001, doi:10.1103/PhysRevLett.115.137001.
[24] J. Zeng, S. Qin, C. Le, J. Hu, Magnetism and superconductivity in the layered hexagonal transition metal pnictides, Phys. Rev. B 96 (2017) 174506, doi:10.1103/PhysRevB.96.174506.
[25] A. Mewis, AB2X2-compounds with $CaAl_2Si_2$ structure. 5. crystal-structure of $CaMn_2P_2$, $CaMn_2As_2$, $SrMn_2P_2$, and $SrMn_2As_2$, Z. Naturforsch. 33 (1978) 606–609 Section ba j. Chem. Sciences, doi:10.1515/znb-1978-0608.
[26] P. Hohenberg, W. Kohn, Inhomogeneous electron gas, Phys. Rev. 136 (1964) B864, doi:10.1103/PhysRev.136.B864.
[27] W. Kohn, L.J. Sham, Self-consistent equations including exchange and correlation effects, Phys. Rev. 140 (1965) A1133, doi:10.1103/PhysRev.140.A1133.
[28] Karlheinz Schwarz, Blaha Peter, Solid state calculations using WIEN2k, Computational Materials Science 28 (2) (2003) 259–273.
[29] J.P. Perdew, K. Burke, M. Ernzerhof, Generalized gradient approximation made simple, Phys. Rev. Lett. 77 (1996) 3865, doi:10.1103/PhysRevLett.77.3865.
[30] P. Guss, M.E. Foster, B.M. Wong, F. Patrick Doty, K. Shah, M.R. Squillante, U. Shirwadkar, R. Hawrami, J. Tower, D. Yuan, Results for aliovalent doping of $CeBr_3$ with Ca^{2+}, J. Appl. Phys. 115 (2014) 034908, doi:10.1063/1.4861647.
[31] H.J. Monkhorst, J.D. Pack, Special points for Brillouin-zone integrations, Phys. Rev. B 13 (1976) 5188, doi:10.1103/PhysRevB.13.5188.
[32] A. Otero-de-la-Roza, D. Abbasi-Pérez, V. Luaña, Gibbs2: A new version of the quasiharmonic model code. II. Models for solid-state thermodynamics, features and implementation, Comput. Phys. Commun. 182 (2011) 2232–2248, doi:10.1016/j.cpc.2011.05.009.
[33] A. Otero-de-la-Roza, V. Luaña, Equations of state and thermodynamics of solids using empirical corrections in the quasiharmonic approximation, Phys. Rev. B 84 (2011) 184103, doi:10.1103/PhysRevB.84.184103.
[34] J.D. Pack, H.J. Monkhorst, Special points for Brillouin-zone integrations"—a reply, Phys. Rev. B 16 (1977) 1748, doi:10.1103/PhysRevB.16.1748.
[35] P. Dai, Antiferromagnetic order and spin dynamics in iron-based superconductors, Rev. Mod. Phys. 87 (2015) 855, doi:10.1103/RevModPhys.87.855.
[36] M. Sahnoun, C. Daul, O. Haas, A. Wokaun, Investigation of the electronic structure in La1− xCaxCoO$_3$ (x= 0, 0.5) using full potential calculations, J. Phys. Condens. Matter 17 (2005) 7995, doi:10.1088/0953-8984/17/50/017.
[37] A. Boochani, H. Khosravi, J. Khodadadi, S. Solaymani, M.M. Sarmazdeh, R.T. Mendi, S.M. Elahi, Calculation of half-metal, debye and curie temperatures of Co_2VAl compound: first principles study, Commun. Theor. Phys. 63 (2015) 641, doi:10.1088/0253-6102/63/5/641.
[38] J. Kübler, G.H. Fecher, C. Felser, Understanding the trend in the Curie temperatures of Co_2-based Heusler compounds: *ab initio* calculations, Phys. Rev. B 76 (2007) 024414, doi:10.1103/PhysRevB.76.024414.
[39] M.E.A. Monir, H. Ullah, H. Baltach, M.G. Ashiq, R. Khenata, Mechanical and magneto-electronic properties of half-metallic ferromagnetism in Ti-doped ZnSe and CdSe alloys: *ab initio* study, J. Magn. Magn. Mater. 442 (2017) 107–117, doi:10.1016/j.jmmm.2017.06.093.
[40] A.T. Petit, P.L. Dulong, Research on some important points of the theory of heat, Ann. Chem. Phys. 10 (1981) 395.
[41] Z. Zada, H. Ullah, R. Zada, A.A. Khan, A. Mahmood, S.M. Ramay, Electronic band profiles, magnetic stability, antiferromagnetic spins ordering and thermodynamics properties of novel antiferromagnet $CaCr_2Sb_2$, Eur. Phys. J. Plus 136 (2021) 1–12, doi:10.1140/epjp/s13360-021-01356-5.
[42] R. Bibi, Z. Zada, A.A. Khan, S. Azam, M. Irfan, B.U. Haq, M. Ahmad, S.A. Khan, First-principles calculations of structural, electronic, magnetic, thermoelectric, and thermodynamic properties of $BaMn_2P_2$ in the anti and ferromagnetic phase, J. Solid State Chem. 302 (2021) 122388, doi:10.1016/j.jssc.2021.122388.
[43] A.A. Khan, Z. Zada, A.H. Reshak, J. Akbar, M. Saqib, M.A. Naeem, M. Ismail, S. Zada, G. Murtaza, A. Laref, M.M. Ramli, Effects of anion-ligands replacement on the structural, electronic and magnetic properties of $ThCo_2X_2$ (X= Si, Ge), Chin. J. Phys. 77 (2022) 956–964, doi:10.1016/j.cjph.2022.03.047.
[44] A.A. Khan, M. Saqib, Z. Zada, F. Chahed, M. Ismail, M. Ishaq, Q. Khan, M. Faizan, Electronic structure, magnetic, and thermoelectric properties of $BaMn_2As_2$ compound: a first-principles study, Phys. Scr. 97 (2022) 065810, doi:10.1088/1402-4896/ac6d1c.
[45] Z. Zada, A.A. Khan, A.H. Reshak, M. Ismail, S. Zada, G. Murtaza, M. Saqib, M.M. Ramli, J. Bila, Cationic variation for $LnAl_2Si_2$ (Ln= Y, Sm, Tb, Dy, Yb) compounds by density functional theory, J. Mol. Struct., 1252 (2022) 132136, doi:10.1016/j.molstruc.2021.132136.
[46] A.A. Khan, A.H. Reshak, Z. Zada, M. Saqib, Z. Abbas, M. Ismail, S. Zada, G. Murtaza, S. Ali, A. Laref, Thermoelectric, structural, electronic, magnetic, and thermodynamic properties of $CaZn_2Ge_2$ compound, Eur. Phys. J. Plus 137 (2022) 1–12, doi:10.1140/epjp/s13360-022-02577-y.
[47] Z. Zada, A.A. Khan, R. Zada, A.H. Reshak, G. Murtaza, M. Saqib, J. Bila, First-principles calculations to investigate variation of cationic-ligand $LmAl_2Ge_2$ (Lm= Ca, Y, La and Ce), Indian J. Phys. (2022) 1–9, doi:10.1007/s12648-021-02242-7.
[48] A.A. Khan, W. Khan, A. Khan, A. Laref, A. Zeb, G. Murtaza, Investigation of the structural, electrical, optical and magnetic properties of $XMg_4Mn_6O_{15}$ (X= K, Rb, and Cs) compounds, Mater. Res. Express 6 (2019) 066102, doi:10.1088/2053-1591/ab07ea.